EEET ECOLOGICAL ENGINEERING & ENVIRONMENTAL TECHNOLOGY

Ecological Engineering & Environmental Technology 2024, 25(9), 328–335
https://doi.org/10.12912/27197050/190162
ISSN 2299–8993, License CC-BY 4.0

Received: 2024.06.03
Accepted: 2024.07.10
Published: 2024.08.01

Latent Heat Fluxes Trend and their Response to El Niño Southern Oscillation at the Global Scale

Abd. Rahman As-syakur[1*]

[1] Marine Science Department, Faculty of Marine and Fisheries, Udayana University, Kampus Bukit Jimbaran, Bali 80361, Indonesia

* Corresponding author's e-mail: ar.assyakur@pplh.unud.ac.id

ABSTRACT

This study employed the Japanese Ocean flux data sets with use of remote sensing observations version 2 (J-OFURO2) to examine global-scale seasonal variations and trends in Latent heat flux (LHF) over a 19-year period. Furthermore, additional analysis has been conducted to determine the response of LHF to the El Niño Southern Oscillation (ENSO) phenomenon. To assess variability, trends, and strength of relationships with ENSO, statistical score analysis was employed using seasonal means, standard deviations, linear trends, and linear correlations, respectively. In this study, the seasons were classified as December-January-February (DJF), March-April-May (MAM), June-July-August (JJA), and September-October-November (SON). The result of the study revealed that the highest LHF values tracked the annual movement of the sun. In the Northern Hemisphere, the highest spatial trends occurred during DJF, while JJA exhibited the peak values in the Southern Hemisphere. This spatial pattern aligns with the seasonal means of LHF, where the highest and lowest standard deviations and trends coincide with the corresponding regions of high and low LHF. This finding suggests that the standard deviation patterns support the observed variability in seasonal LHF means. The strongest spatial correlations between LHF and ENSO were observed over the Indian Ocean during the SON season. In contrast, the correlations between LHF and ENSO in the Atlantic Ocean exhibited spatial heterogeneity, with a significant correlation only during the DJF season. In general, the seasonal spatio-temporal patterns suggest a dynamic link between LHF and ENSO, potentially linked to large-scale monsoon system changes, the specific locations and distributions of positive/negative trends and standard deviations in LHF reveal a spatial response that appears independent of the ENSO phenomenon.

Keywords: heat flows, climate change, seasonal variability, spatial variability, satellite-based estimation.

INTRODUCTION

The exchange of heat fluxes across the air-sea interface significantly impacts both the ocean and atmosphere (Liu and Zhou, 2018). LHF, the most variable component on monthly and longer scales across vast ocean regions (Liu, 1988), depends primarily on a few ocean-atmosphere parameters like air-sea moisture difference and wind speed (Yu et al., 2007). These factors vary with time scale and location. For example, long-term LHF trends are primarily driven by tropical Pacific sea surface temperature and wind speed (Li et al., 2011; Yang et al., 2016). LHF refers to the energy transfer rate, either absorbed or released, during a phase transition of a substance, whilst maintaining a constant temperature (Liou et al., 2018). Studies in the Pacific Ocean suggest that ENSO modulates LHF variability through its influence on sea surface temperature (SST) and wind speed (e.g., Liu and Zhou, 2018).

The main energy loss for the oceans and the main energy source for many processes in the atmosphere is LHF (Crewell et al., 1991), a key component of the hydrological cycle (Chou et al., 2004). Investigating LHF variability at the global scale and its response to ENSO is important for understanding the global hydrological cycle, energy balance, and climate change (Li et al., 2011). Studies of LHF characteristics especially in terms

of its intensity distribution in different temporal and spatial domains are imperative to quantifying the impact of climate change based on decreasing/increasing trend for the different intensity. The major intraseasonal LHF variability is due to winds, but spatial variability of humidity and SST are also important (Grodsky et al., 2009). A positive trend in LHF is associated with a positive trend in surface wind speed (Liu and Curry, 2006). Additional trends in SST are marked by large interannual variations associated with ENSO (Yu and Weller, 2007).

The ENSO is the largest and best known mode of climate variability that affects weather, ecosystems and societies in large parts of the world (van Oldenborgh et al., 2005; Ashok and Yamagata, 2009). ENSO contributes to global air-sea interaction anomalies through teleconnections – changes in the Walker and Hadley circulations, oceanic Kelvin and Rossby waves, 'atmospheric bridge' mechanisms, and atmospheric Rossby wave trains (Curtis, 2008). The ENSO-driven large-scale atmospheric teleconnections alter the near-surface air temperature, humidity, and wind, as well as the distribution of clouds (Alexander et al., 2002). Globally, ENSO has affected the variability of environment variable such as rainfall and evaporation (Ropelewski and Halpert, 1987; Enfield and Mestas-Nuñez, 2000). Previous studies have found correlations between ENSO and LHF, such as in tropical Pacific (Congbin et al., 1992), and South China Sea (Zong et al., 2010). However, studies of the global response of remote sensing LHF to ENSO phenomenon not yet carried out. For that reason, understanding the global patterns of ENSO-induced LHF is important for evaluating climate models and ENSO-related forecasts of atmospheric processes.

Ocean surface heat flux displays high space–time variability that requires frequent observations for adequate representation. Global air-sea heat flux data sets which have higher spatial-temporal resolution can be obtained from satellite observations, including LHF, other than model-derived datasets or in-situ measurements. One dataset that employs satellite observation is the Japanese Ocean Flux Data Sets using Remote Sensing Observations (J-OFURO). J-OFURO data sets have three versions, J-OFURO1, J-OFURO2, and J-OFURO3 constructed by Kubota et al. (2002), Kubota et al. (2006), and Tomita et al. (2019), respectively. J-OFURO1 had errors due to inaccuracies in the satellite-based humidity and air temperature state variables (Tomita and Kubota, 2006) which have been repaired in J-OFURO2, including multi-satellite data and change in gridded SST (Kubota et al., 2006). Even though J-OFURO3 has been developed, the bias value is relatively similar to J-OFURO2 (Tomita et al., 2021). In previous studies, comparisons show good agreement J-OFURO2 LHF with in situ LHF (Tomita et al., 2010; Iwasaki et al., 2010; Kubota et al., 2010). Comparison with various LHF data derived from remote sensing also demonstrates relatively quite good bias values (Tomita et al., 2019).

The main objectives of this paper are to identify patterns of LHF variability and trends using J-OFURO2 datasets over the period 1988–2006, with a particular focus on potential links to the ENSO phenomenon. This study defines ENSO conditions by the Nino3.4 index (Trenberth, 1997) and uses mainly seasonal analysis. This study is expected to generate more comprehensive spatial information on LHF variability and trends, as well as their relationship to ENSO, due to its global analysis, whereas previous studies were conducted in separate regions, such as the Pacific Ocean (Baosen, 1989) or Indian Ocean (Swain and Ghose, 2020). In addition, ENSO events are now occurring more frequently and with greater intensity, suggesting that climate change is escalating in severity, which will have a substantial impact on the LHF variability and global environment.

DATA AND METHOD

Monthly-mean global ocean surface LHF data for the period from 1988 to 2006, measured and collected by J-OFURO2 (version 2), were used to analyse the spatial variability and the relationship with ENSO. Monthly-mean LHF values are based on daily-mean values of LHF produced by J-OFURO2. J-OFURO2 was only available for 19 years from January 1988 to December 2006. Nino3.4 values were used to determine warm (El Niño) and cold (La Niña) events in the Pacific Ocean (Trenberth, 1997). The Nino3.4 index, which can be considered as the atmospheric manifestation of the ENSO, is defined as the spatial mean SST anomaly over the 5°N–5°S and 170–120°W region of the Pacific Ocean.

Multi-satellite and sensor data from J-OFURO2 are constructed from SST, surface wind

speed, and surface air specific humidity (Kubota et al., 2006; Kubota and Tomita, 2007; Kubota et al., 2010). For SST, J-OFURO2 uses Merged satellite and in situ data Global Daily Sea Surface Temperatures (MGDSST) provided by Japan Meteorological Agency (JMA). The MGDSST data set has been created by using infrared radiation SSTs (National Oceanic and Atmospheric Administration (NOAA)/Advanced Very High Resolution Radiometer (AVHRR)), Microwave SSTs (Aqua/Advanced Microwave Scanning Radiometer – Earth observing system (Aqua/AMSR-E)) and in-situ data (Sakurai et al., 2005). Furthermore, surface wind speed is constructed from a combination of microwave radiometers, i.e., Defense Meteorological Satellite Program (DMSP)/ Special Sensor Microwave Imager (SSMI) F08, F10, F11, F13, F14, F15, Aqua/AMSR-E, Tropical Rainfall Measurement Mission (TRMM)/TRMM Microwave Imager (TMI), and microwave scatterometers (European Resource Sensing (ERS)/ Active Microwave Instrument (AMI) and QuikScat/SeaWinds). Meanwhile, for surface air specific humidity, J-OFURO2 uses only available data from the DMSP/SSMIs sensors (i.e., F08, 10, 11, 13, and 14). Finally, a bulk algorithm used for estimation of LHF changed from Kondo (1975) for J-OFURO1 to COASRE 3.0 (Fairall et al., 2003) for J-OFURO2. These products are unified to the daily and monthly averaged data of 1° grids.

Statistical scores analysis of LHF spatial variability and Nino3.4 value relationships use seasonal means and standard deviations, while linear slope determines LHF trends. The linear correlation coefficient (r) measured the closeness of LHF estimates to Niño3.4 index values. Correlation is used to describe a linear statistical relationship between two random variables, in which a pair of variables vary together precisely, i.e., one variable is related to the other by means of a positive or negative scaling factor (von Storch and Zwiers, 1999), which were defined as follows:

$$r = \frac{n\sum XY - \left(\sum X\right)\left(\sum Y\right)}{\sqrt{n\sum X^2 - \left(\sum X\right)^2} \times \sqrt{n\sum Y^2 - \left(\sum Y\right)^2}} \quad (1)$$

where: X is the LHF from J-OFURO2 values, Y is the Nino3.4 index values, and n the number of data pairs.

Seasonal analysis, based on annual sun movement, of monthly seasonal data across different years was primarily used for this research. Analysis was conducted in each pixel, using coordinates for identity. Point-by-point data for each pixel was extracted from the J-OFURO, including coordinates, month, year, and LHF values. Then, data sets were averaged in accordance with the purpose of the analysis. This averaging process was also performed on Niño3.4 index values, followed by the calculation of seasonal means, standard deviations, linear slope, and the linear correlation coefficients. After obtaining calculation values, the point data was converted into a raster data format with the same spatial resolution as the original data (1° × 1°). The year was divided into the following four seasons: DJF, MAM, JJA, and SON.

RESULTS AND DISCUSSIONS

Seasonal spatial patterns of LHF variability, based on mean composites, are presented in Figure 1. Equatorial region LHF values were lower than low-latitude storm track region LHF values in all seasons. Generally, maximum and minimum LHF values were related to patterns of annual sun movement, however, minimum values appeared in high latitudes and a small part of Tropical Pacific on the western coast of Peru and Ecuador. During DJF season, the LHF in the northern Hemisphere was generally somewhat higher than that in the southern Hemisphere. The highest values of LHF (> 200 W m^{-2}) appeared over the west Pacific and west Atlantic in the north Hemisphere, while the lowest values (< 15 W m^{-2}) were found in the southern oceans. Polar high LHF values were observed over the north and south Indian Ocean, with a similar case also found in the Atlantic Ocean. High values of LHF continued moving towards the southern Hemisphere during MAM season, coinciding with a disappearance of the highest LHF values over the west Pacific in the North Hemisphere and a rise of two high LHF belts over the low-latitude storm track region in the north and south Hemisphere, while the lowest LHF values manifested in the north Hemisphere. During JJA season, the highest values of LHF occurred over east Pacific and west Indian Oceans in the southern Hemisphere, in contrast to the DJF season. Wide areas of minimum LHF values were observed in the north Hemisphere of the Pacific and Atlantic Oceans. The lowest values of LHF faded during the SON season over the north Hemisphere. Finally, large areas of high LHF values returned, moving to northern Hemisphere low-latitude storm track regions.

Figure 2 illustrates spatial patterns of seasonal standard deviations based on mean composites

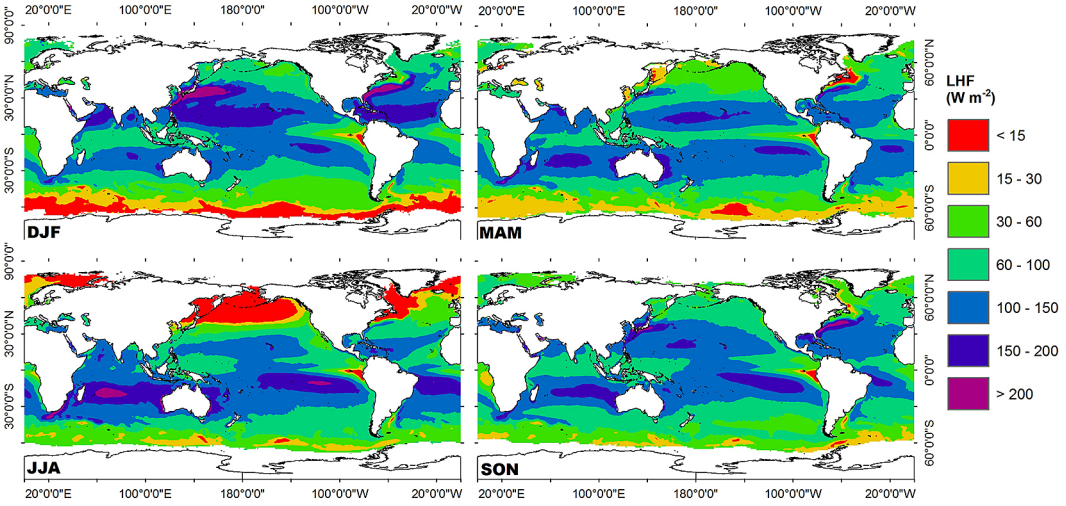

Figure 1. Spatial pattern seasonal mean of LHF based on monthly composites of the same season from January 1988 to December 2006

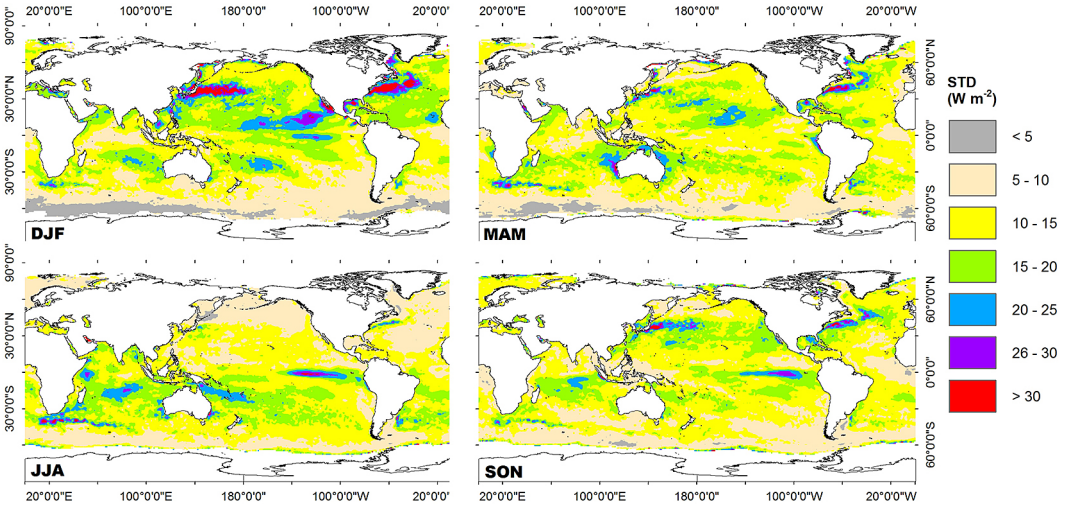

Figure 2. Distribution of standard deviation of seasonal averaged LHF from J-OFURO2 data

of LHF from J-OFURO2 data. The standard deviation is the square root of the averaged squared deviations from the mean (Brown, 1982). Standard deviations are informative for the data distribution of nearly all the recorded data (Gravetter and Wallnau, 2006). Higher/lower standard deviations indicate larger/smaller seasonal variability. Highest standard deviation values (> 30 W m^{-2}) occurred during the DJF season in the western Pacific and Atlantic Oceans over the northern Hemisphere, a similar location to the highest values of the LHF seasonal mean. The smallest LHF standard deviation was found over the sub tropic region. Generally, location of the highest and lowest standard deviation values corresponds to the seasonal mean of LHF values, supporting the seasonal mean LHF variability. Yu and Weller (2007) explained the standard deviation of LHF is primarily caused by sea-air specific humidity and temperature differences, whereas wind speed plays a minor role.

The spatial presentation of detected LHF trends are useful for better understanding the variations of global LHF. Seasonal trends in global LHF for the period 1988–2006 is presented in Figure 3. Generally, the positive trend area is wider than negative trend areas. Most high positive trend was detected over north Hemisphere, except for the JJA season observed in the south Hemisphere. Additionally, the highest positive trend was predominantly found in regions with the highest values of LHF seasonal mean (Figure 1) and standard deviation (Figure 2) across all seasons. The positive and negative LHF trends are

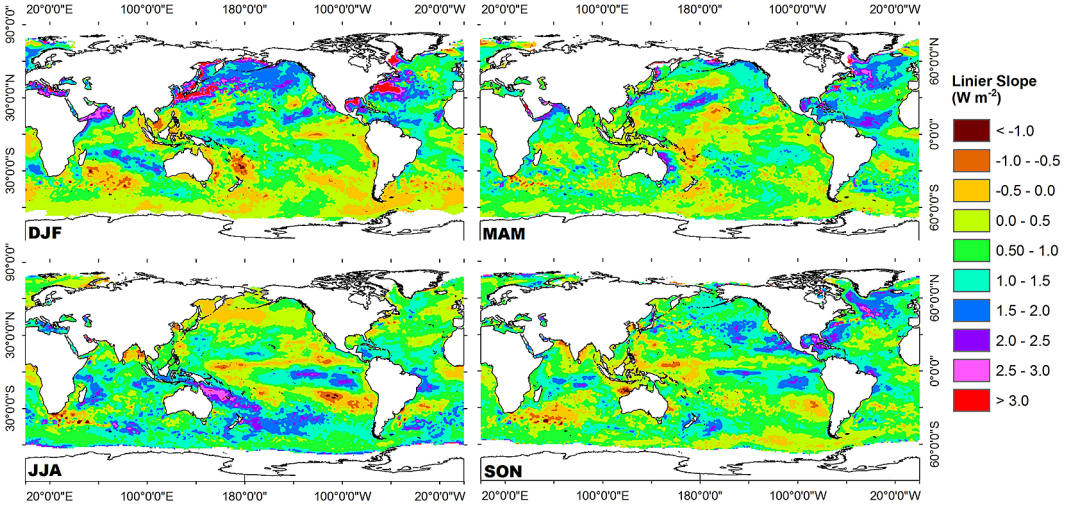

Figure 3. Spatial-distribution trend of LHF for each season derived from the J-OFURO2

closely associated with both sea surface temperature and surface wind speed trends, as explained by Good et al. (2007) and Zheng et al. (2013).

Figure 4 shows seasonal spatial pattern relationships of LHF with ENSO for the period 1988–2006. Generally, the ENSO impact on LHF consistently occurs over the tropical Pacific in all seasons. These findings generally agree with Congbin and Diaz (1992) who state that the interannual variability of LHF over the tropical Pacific exhibits strong correlation with ENSO phenomena. A negative impact of Nino3.4 values on LHF are detected over the northern Atlantic and tropical Pacific in the western and south hemisphere of the Indian and Atlantic Oceans for the DJF season. Additionally, positive correlations are inspected over the eastern tropical Pacific, and northern Pacific in the west. The effect of spatial distribution of ENSO on LHF fluctuation is smaller during MAM season compared to DJF season. Most negative responses of LHF to ENSO are observed in the southern Hemisphere over eastern Pacific and Indian Oceans as well as over the tropical Atlantic in the west. Meanwhile, a positive correlation is found over tropical Pacific area. Spatial pattern responses between LHF and ENSO during JJA seasons can be seen clearly over the tropical Pacific, with two polar clusters, negative in the west and positive in east. The LHF shows a negative correlation with ENSO in the southern Atlantic and Pacific Ocean, while it displays a positive correlation over the north Pacific and Maritime Continent. During the SON season, two polar spatial cluster correlations were still observed in the tropical Pacific. Negative impacts of ENSO and LHF appeared over southern Hemisphere and

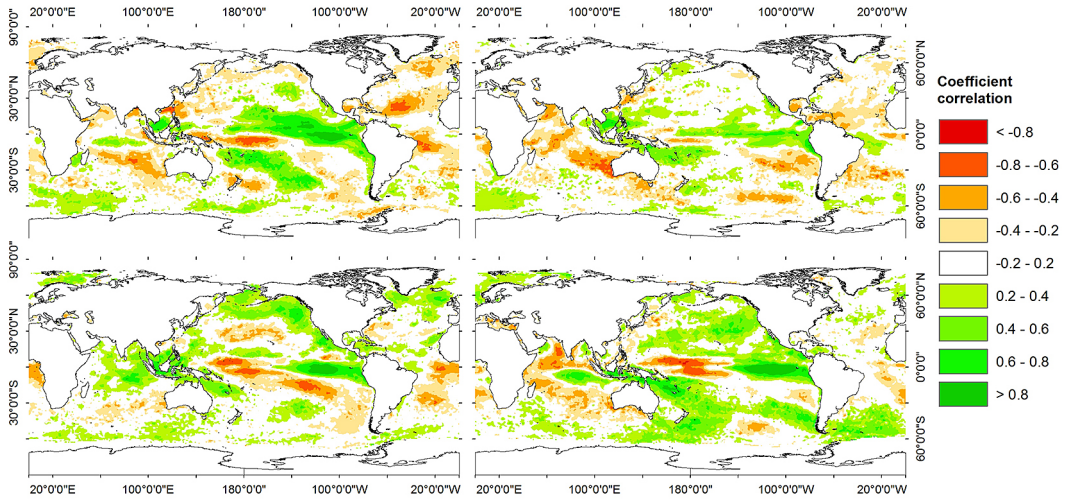

Figure 4. Seasonal analysis of the linear spatial correlations between Nino 3.4 index and LHF in each grid

northern Indian Ocean. Meanwhile, a positive relationship became visible over south Pacific in the east and north Pacific in the west. However, when comparing the spatial pattern of the LHF response to ENSO with the positive and negative LHF trends and the distribution of standard deviations, it was indicated that the location was unrelated to the spatial distribution relationships between LHF and ENSO. This may indicate that the LHF trends are independent of the ENSO phenomenon. Nevertheless, this evidence requires additional investigation using extended datasets and other complementary data sources that contribute to the development of LHF, including SST and wind speed.

CONCLUSIONS

An investigation of 19 years (January 1988–December 2006) of global LHF variability and ENSO relationships using J-OFURO2 data is presented here. The results revealed a highest LHF values tracking the annual movement of the sun, with the clear association between high LHF and seasonal storm tracks. The spatial distributions of trends showed peak values in the Northern Hemisphere during DJF and in the Southern Hemisphere during JJA. This pattern matches the seasonal means and standard deviation of LHF, where regions of high and low LHF correspond to the highest and lowest LHF trends. The spatial patterns suggested a dynamic movement of the relationship between ENSO and LHF, generally linked to the variations in the sun movement system across the entire ocean. The spatial responses of LHF to ENSO have different patterns in each Ocean region. Most of the Pacific Ocean response to ENSO appeared during SON, DJF and JJA. The highest spatial correlations between LHF and ENSO occurred over the Indian Ocean in the SON season. Additionally, uneven correlations occurred between LHF and ENSO in the Atlantic Ocean, except in the DJF season.

Future research efforts should focus on a more comprehensive understanding of the LHF-ENSO relationship using extended datasets, such as using J-OFURO3 for which data is available until 2017 and will continue to be updated. Given the possibility that LHF variability and trends may not be related to ENSO, further evidence is required. Additionally, investigating the link between LHF and other global climate phenomena, such as the Indian Ocean Dipole (IOD), is necessary to achieve a holistic comprehension of its influence on climate change.

Acknowledgements

We gratefully acknowledge the data received from the following organizations: J-OFURO data from the School of Marine Science and Technology, Tokai University; and Nino3.4 index data from the National Oceanic and Atmospheric Administration (NOAA) Center for Weather and Climate Prediction.

REFERENCES

1. Alexander, M.A., Bladé, I., Newman, M., Lanzante, J.R., Lau, N.C., Scott, J.D. 2002. The atmospheric bridge: The influence of ENSO teleconnections on air-sea interaction over the global oceans. Journal of Climate, 15(16), 2205–2231. https://doi.org/10.1175/1520-0442(2002)015<2205:TABTIO>2.0.CO;2
2. Ashok, K., Yamagata, T. 2009. The El Niño with a difference. Nature, 461, 481–484. https://doi.org/10.1038/461481a
3. Baosen, L. 1989. The latent and sensible heat fluxes over the western tropical Pacific and its relationship to ENSO. Advances in atmospheric sciences, 6(4), 467-474, https://doi.org/10.1007/BF02659080
4. Brown, G.W. 1982. Standard deviation, standard error: Which'standard'should we use?. American Journal of Diseases of Children, 136(10), 937–941.
5. Chou, S-H., Nelkin, E., Ardizzone, J., Atlas, R.M. 2004. A Comparison of latent heat fluxes over global oceans for four flux products. Journal of climate, 17, 3973–3989. https://doi.org/10.1175/1520-0442(2004)017<3973:ACOLHF>2.0.CO;2
6. Congbin, F., Diaz, H., Huijun, F. 1992. Variability in latent heat flux over the tropical pacific in association with recent two ENSO events. Advances in atmospheric sciences, 9(3), 351–358. https://doi.org/10.1007/BF02656945
7. Crewell, S., Ruprecht, E., Simmer, C. 2009. Latentheat flux over the north atlantic ocean - A case study. Journal of applied meteorology, 30, 1627–1635. https://doi.org/10.1175/1520-0450(1991)030<1627:LHFOTN>2.0.CO;2
8. Curtis, S. 2008. The El Niño–Southern Oscillation and Global Precipitation. Geography Compass, 2/3, 600–619. https://doi.org/10.1111/j.1749-8198.2008.00105.x
9. Enfield, D.B., Mestas-Nuñez, A.M. 2000. Global

modes of ENSO and non-ENSO sea surface temperature variability and their associations with climate. in Diaz, H.F., and Markgraf, V. (Eds). El Niño and the Southern Oscillation: multiscale variability and global and regional impacts. Cambridge University Press, Cambridge, UK, 89–112.

10. Fairall, C.W., Bradley, E.F., Hare, J.E., Grachev, A.A., Edson, J.B. 2003. Bulk parameterization of airsea fluxes: Updates and verification for the COARE algorithm. Journal of climate, 17, 571–591. https://doi.org/10.1175/1520-0442(2003)016%3C0571:BPOASF%3E2.0.CO;2
11. Good, S.A., Corlett, G.K., Remedios, J.J., Noyes, E.J., Llewellyn-Jones, D.T. 2007. The global trend in sea surface temperature from 20 years of advanced very high resolution radiometer data. Journal of climate, 20(7), 1255–1264. https://doi.org/10.1175/JCLI4049.1
12. Gravetter, F., and Wallnau, L. 2006. Statistics for the behavioral sciences, 8th edition. Wadsworth, Cengage Learning. Belmont, California, USA.
13. Grodsky, S.A., Bentamy, A., Carton, J.A., Pinker, R.T. 2009. intraseasonal latent heat flux based on satellite observations. Journal of climate, 22, 4539–4556. https://doi.org/10.1175/2009JCLI2901.1
14. Kondo, J. 1975. Air-sea bulk transfer coefficients in diabatic conditions. Boundary-Layer Meteorology, 9(1), 91–112. https://doi.org/10.1175/1520-0442(1999)012%3C0917:RSSTVD%3E2.0.CO;2
15. Kubota, M., Tomita, H. 2007. Introduction of J-OFURO latent heat flux version 2, in: Proceedings of the Joint 2007 EUMETSAT Meteorological Satellite Conference and the 15th Satellite Meteorology and Oceanography Conference of the American Meteorological Society, Amsterdam, The Netherlands, 24–28 September.
16. Kubota, M., Tomita, H., Iwasaki, S. 2006. Introduction of J-OFURO version 2. In 36th COSPAR Scientific Assembly 36, 2297). Held 16–23 July 2006, in Beijing, China. COSPAR2006-A-02297
17. Kubota, M., Kano, A., Muramatsu, H., Tomita, H. 2003. Intercomparison of various surface latent heat flux fields. Journal of climate, 16(4), 670–678. https://doi.org/10.1175/1520-0442(2003)016%3C0670:IOVSLH%3E2.0.CO;2
18. Kubota, M., Iwasaka, N., Kizu, S., Konda, M., Kutsuwada, K. 2002. Japanese ocean flux data sets with use of remote sensing observations (J-OFURO). Journal of Oceanography, 58(1), 213–225. https://doi.org/10.1023/A:1015845321836
19. Kubota, M., Hiroyuki, T., Kutsuwada, K., Akiyama, M., Iwasaki, S. 2010. Introduction of Japanese Ocean Flux data sets with Use of Remote sensing Observations (J-OFURO) Version 2 in Proceedings of OceanObs'09: Sustained Ocean Observations and Information for Society (Annex), Venice, Italy, 21–25 September 2009, Hall, J., Harrison, D.E., Stammer, D., Eds., ESA Publication WPP-306, doi:10.5270/OceanObs09
20. Li, G., Ren, B., Yang, C., Zheng, J. 2011. Revisiting the trend of the tropical and subtropical Pacific surface latent heat flux during 1977–2006. Journal of Geophysical Research: Atmospheres, 116, D10115, https://doi.org/10.1029/2010JD015444
21. Liou, Y.A., Le, M.S., Chien, H. 2018. Normalized difference latent heat index for remote sensing of land surface energy fluxes. IEEE Transactions on Geoscience and Remote Sensing, 57(3), 1423-1433, https://doi.org/10.1109/TGRS.2018.2866555
22. Liu, J., Curry, J.A. 2006. Variability of the tropical and subtropical ocean surface latent heat flux during 1989–2000. Geophysical Research Letters, 33, L05706-1–L05706-5. https://doi.org/10.1029/2005GL024809
23. Liu, W.T. 1988. Moisture and latent heat flux variabilities in the tropical Pacific derived from satellite data. Journal of Geophysical Research: Oceans, 93(C6), 6749–6760, https://doi.org/10.1029/JC093iC06p06749
24. Liu, Z., Zhou, L.T. 2018. Evolution features of the surface latent heat flux anomalies over the tropical Pacific associated with two types of ENSO events. Theoretical and Applied Climatology, 134, 721–737, https://doi.org/10.1007/s00704-017-2264-9
25. Ropelewski, C.F., Halpert, M.S. 1987. Global and regional scale precipitation patterns associated with the El Niño/Southern Oscillation. Monthly weather review, 115(8), 1606–1626. https://doi.org/10.1175/1520-0493(1987)115%3C1606:GARSPP%3E2.0.CO;2
26. Sakurai, T., Yukio, K., Kuragano, T. 2005. Merged satellite and in-situ data global daily SST. In Geoscience and Remote Sensing Symposium, 2005. IGARSS'05. Proceedings. 2005 IEEE International, 4, 2606–2608. https://doi.org/10.1109/IGARSS.2005.1525519
27. Swain, D., Ghose, S.K. 2020. Latent and Sensible heat flux variation in north Indian Ocean during ENSO and Indian Ocean dipole years. In IEEE 2020 XXXIIIrd General Assembly and Scientific Symposium of the International Union of Radio Science, 1–3. https://doi.org/10.23919/URSIGASS49373.2020.9232005
28. Tomita, H., Kubota, M. 2006. An analysis of the accuracy of Japanese Ocean Flux data sets with Use of Remote sensing Observations (J-OFURO) satellite-derived latent heat flux using moored buoy data. Journal of Geophysical Research: Oceans, 111(C7), https://doi.org/10.1029/2005JC003013
29. Tomita, H., Kubota, M., Cronin, M.F., Iwasaki, S., Konda, M., Ichikawa, H. 2010. An assessment of

surface heat fluxes from J-OFURO2 at the KEO and JKEO sites. Journal of Geophysical Research, 115, C03018-1– C03018-13. https://doi.org/10.1029/2009JC005545

30. Tomita, H., Hihara, T., Kako, S. I., Kubota, M., Kutsuwada, K. 2019. An introduction to J-OFURO3, a third-generation Japanese ocean flux data set using remote-sensing observations. Journal of Oceanography, 75(2), 171–194, https://doi.org/10.1007/s10872-018-0493-x
31. Tomita, H., Kutsuwada, K., Kubota, M., Hihara, T. 2021. Advances in the estimation of global surface net heat flux based on satellite observation: J-OFURO3 V1. 1. Frontiers in Marine Science, 8, 612361. https://doi.org/10.3389/fmars.2021.612361
32. Trenberth, K.E. 1997. The definition of El Niño. Bulletin of the American Meteorological Society, 78:2771–2777. https://doi.org/10.1175/1520-0477(1997)078%3C2771:TDOENO%3E2.0.CO;2
33. van Oldenborgh, G.J., Philip, S.Y., Collins, M. 2005. El Niño in a changing climate: a multi-model study. Ocean Science, 1, 81–95. https://doi.org/10.5194/os-1-81-2005
34. von Storch, H., Zwiers, F.W. 1999. Statistical Analysis in Climate Research. Cambridge University Press, 484: Cambridge, UK.
35. Yang, H., Liu, J., Lohmann, G., Shi, X., Hu, Y., Chen, X. 2016. Ocean-atmosphere dynamics changes associated with prominent ocean surface turbulent heat fluxes trends during 1958–2013. Ocean Dynamics, 66, 353–365, https://doi.org/10.1007/s10236-016-0925-3
36. Yu, L., Weller, R.A. 2007. Objectively analyzed air–sea heat fluxes for the global ice-free oceans (1981–2005). Bulletin of the American Meteorological Society, 88, 527–539. https://doi.org/10.1175/BAMS-88-4-527
37. Yu, L., Jin, X., Weller, R.A. 2007. Annual, seasonal, and interannual variability of air–sea heat fluxes in the Indian Ocean. Journal of climate, 20(13), 3190–3209, https://doi.org/10.1175/JCLI4163.1
38. Zheng, C., Zhou, L., Huang, C., Shi, Y., Li, J., Li, J. 2013. The long-term trend of the sea surface wind speed and the wave height (wind wave, swell, mixed wave) in global ocean during the last 44 a. Acta Oceanologica Sinica, 32(10), 1–4. https://doi.org/10.1007/s13131-013-0358-5
39. Zong, H., Liu, Y., Xiu, P., Xu, Q., Rong, Z. 2010. Interannual variability of latent and sensible heat fluxes in the South China Sea. Chinese Journal of Oceanology and Limnology, 28, 153–159. https://doi.org/10.1007/s00343-010-9241-9